A Robust and Simple Patient-derived Multicellular Spheroid Model Enables Liver Cancer Precision Drug Screening

Sara Cherradi
Université de Strasbourg, INSERM U1110
Nuno Almeida
Universite de Strasbourg 1: Universite de Strasbourg
Antonio Saviano
Université de Strasbourg, INSERM U1110
Sarah Durand
Université de Strasbourg, INSERM U1110
Emanuele Felli
CHU Strasbourg: Hopitaux universitaires de Strasbourg
Patrick Pessaux
CHU Strasbourg: Hopitaux universitaires de Strasbourg
Catherine Schuster
Université de Strasbourg, INSERM U1110
Thomas Baumert
Université de Strasbourg, INSERM U1110
Hong Tuan Duong (f.duong@unistra.fr)
Université de Strasbourg, INSERM U1110

Research Article

Keywords: personalized care, liver cancer, preclinical drug response testing

Posted Date: February 11th, 2021

DOI: https://doi.org/10.21203/rs.3.rs-183605/v1

A robust and simple patient-derived multicellular spheroid model enables liver cancer precision drug screening (111 characters)

Category. Technical advances and resources

Authors. Sara Cherradi[1], Nuno Almeida[1], Antonio Saviano[1,2], Sarah Durand[1], Emanuele Felli[1,2,3], Patrick Pessaux[1,2,3], Catherine Schuster[1], Thomas F. Baumert[1,2,#,*], & Hong Tuan F. Duong[1,#].

Affiliations. [1]Université de Strasbourg, Inserm, Institut de Recherche sur les Maladies Virales et Hépatiques UMR_S1110, Strasbourg, France; [2]Institut Hospitalo-Universitaire; [3]Service de chirurgie viscérale et digestive, Pôle Hépato-digestif, Nouvel Hôpital Civil, Strasbourg, France.

# these authors contributed equally.

*Correspondence to: Prof. Thomas F. Baumert, MD, Inserm U1110, University of Strasbourg, 3 Rue Koeberlé, F-67000 Strasbourg. Phone: +33368853703, email: thomas.baumert@unistra.fr

Keywords: personalized care, liver cancer, preclinical drug response testing

Conflict of interest. The authors have declared that no conflict of interest exists.

Summary. Tailoring a treatment protocol to individual patient needs a robust system that could be used to monitor the preclinical drug response. We establish a model that fulfills these requirements helping to accelerate the clinical research program for personalized medicine.

Author contributions. S.C., N.U., H.T.D. performed the experiments. S.D., A.S., C.S. organized the collection of liver tissues. E.F., P.P. provided liver tissues. H.T.D., T.B. conceptualized and wrote the manuscript. H.T.D., S.C. analyzed the data

Acknowledgements.

The authors thank the Centre de Ressources Biologiques-Biological Resource Centre, Strasbourg, France, for the management of patient-derived liver tissues.

Financial support. This work is supported by the European Union (H2020 HEPCAR #667273, ERC PoC-HEPCAN #862551 to TFB). ARC, Paris and Institut Hospitalo-Universitaire, Strasbourg (TheraHCC and TheraHCC2.0 IHUARC IHU201301187 and IHUC201901299 TFB). This work has been published under the framework of the LABEX ANR-10-LABX-0028_HEPSYS and PLAN CANCER 2014-2019 HCCMICTAR and benefits from a funding from the state managed by the French National Research Agency as part of the Investments for the Future Program, INCa (National Institute for Cancer) and INSERM.

Abstract. (164 words**)**

Background & Purpose. Hepatocellular carcinoma (HCC) is the second leading and fastest rising cause of cancer death worldwide. HCC is often diagnosed when it is not curable. Thus, there are many challenges associated with the treatment of HCC. Until now there is no simple and robust system for reliable pre-treatment screening of approved drugs.

Methods. We developed a simple and robust patient-derived multicellular cell clustering model from 18 liver resections. We applied this technology on 9 HCC liver tissues and assessed FDA-approved drug responses.

Results. The success rate of our model is 100% independently from the type of liver underlying disease. The model shows differential responses to HCC targeted- and immune-based treatments with a high reproducibility. Our work highlights that preserving the integrity of the primary liver architecture permits to perpetuate the physiopathology.

Conclusion. This model system will help to understand the biological role of the tumor microenvironment and to accelerate the clinical research program for personalized liver cancer treatment based on functional screening.

Graphical abstract.

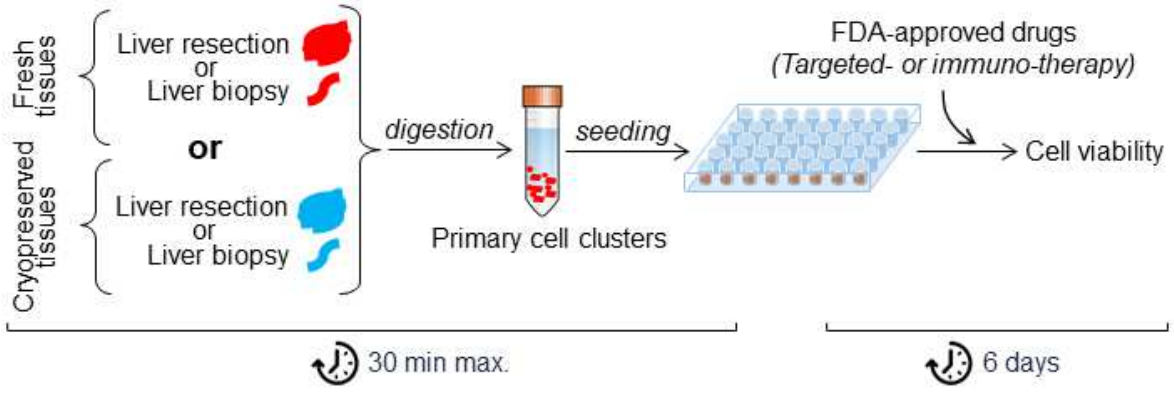

Introduction.

Liver cancer is the fifth most common cancer and the second most frequent cause of cancer-related death worldwide (1). Current therapeutic options are limited by a response rate of less than 30% and often exhibit severe adverse effects that lead to the discontinuation of the treatment (2). The absence of accurate predictive models makes impossible the right decision-making process in which a patient is enrolled in a treatment protocol (3). Several strategies were proposed to explore ways to fast-track drug screening. However, extended culture of cell lines can lead to secondary genomic changes that modify their response/behavior to anticancer drugs (4). Organoids must be grown by stem cells through a complex induction process that hampers the success rate of organoid cultures (5). Their growth relies on rigid extracellular matrices that create biochemical forces on cells reducing drug penetration (6). Organoids are epithelial cultures that lack tumor stroma, thus they do not allow drug testing that target host–tumor interactions (7). The establishment of patient-derived xenograft (PDX) models is time consuming and not all tumor tissues are suitable (8). Moreover, PDX mice lacked the immune system and a murine-specific tumor evolution may occur (9).

We established a heterogeneous and functional patient-derived model for drug screening in individual patients. We show that the model is successful for studying drug treatment responses including cancer cell targeted- and immune-based therapies. We report a high intra-individual reproducibility of the drug response.

Materials and methods.

Human subjects and liver tissue collection.

Resected tissues are from the Centre Hospitalier Universitaire (CHU) of Strasbourg. They were stored in HypoThermosol FRS Preservation Solution (Sigma-Aldrich) and kept at +4°C prior processing or cryopreserved at -80°C in CryoStor® cell cryopreservation media (Sigma-Aldrich). The protocols were approved by the Ethics Committee of the Strasbourg University Hospitals (DC-2016–2616). Written and informed consent was obtained from all patients.

Generation of patient-derived spheroids.

Resected liver tissues (5x5mm to 8x8mm size) were chopped in small fragments and digested with a 0.05% collagenase-EGTA solution followed by a gentle mechanical disruption and size filtering with a 70µM strainer, to generate aggregates of cells. Aggregates are assembled into spheroids Corning® 96-well Black/Clear Bottom Low Flange Ultra-Low Attachment Microplate (Corning) and cultured in MammoCult™ Basal Medium supplemented with MammoCult™ Proliferation supplement, Heparin, Hydrocortison (all from STEMCELL™ Technologies), Penicillin/Streptomycin, Fungizone, FBS (from GIBCO), and Primocin (InvivoGen). The full process should not last longer than 30 minutes.

For cryopreserved liver tissues, resected liver tissues were thawed in a +37°C water bath prior processing as described above.

FDA-approved drug treatments.

Sorafenib tosylate (10µM), lenvatinib (10µM), regorafenib (10µM), cabozantinib (10µM), nivolumab (10µg/ml), atezoluzimab (10µg/ml), and bevacizumab (10µg/ml) were from Selleckchem. Tumorspheres were treated for 6 days.

Cell viability assay.

Cell viability was performed using CellTiter3D Glo (Promega). Results are expressed as RLUs mean ± s.d. or as percentage to control mean ± s.d. A minimum of three replicates were performed for each culture or treatment condition.

Albumin and CYP3A4 activity.

Albumin release was measured by ELISA (Bethyl Laboratories) and CYP3A4 activity was determined using CYP3A4 Activity Assay Kit (Abcam).

MIP1a/CCl3, triglyceride, and total collagen deposition.

MIP1a/CCl3 was measured by ELISA using Human MIP1a ELISA Kit (Abcam). Triglycerides content was analyzed using Triglyceride Assay Kit (Abcam). Total collagen was quantified using Total Collagen Assay Kit (Abcam).

Actin cytoskeleton and focal adhesion staining.

Patient-derived spheroids were transferred onto glass chamber slide. Actin cytoskeleton and FAK were visualized using the Actin Cytoskeleton & Focal Adhesion Staining Kit (Sigma-Aldrich). The kit consists of TRITC-conjugated phalloidin, anti-Vinculin, and DAPI for the immunofluorescence staining of actin filaments in the cytoskeleton as well as the nuclei.

Immunofluorescence.

Patient-derived spheroids were transferred onto glass chamber slide. The procedure for immunofluorescence used is a standard protocol for cell cultures described elsewhere. Briefly, cells were fixed with formaldehyde, permeabilized with Triton-100, blocked with BSA, and incubated for overnight with E-cadherin, CD14, or αSMA specific antibodies (Cell Signaling). Cells were visualized by confocal microscopy.

Statistics.

ANOVA Post Hoc Fisher's LSD, with multiple comparisons was performed using GraphPad Prism 7.0, *** $p<0.001$, ** $p<0.01$, * $p<0.05$.

Results.

A simple and robust protocol to establish a patient-derived multicellular spheroids. A workflow was setup to generate patient-derived spheroids using diseased liver tissues (Fig. 1a). All liver tissues obtained from patients enrolled in this study and their clinical characteristics are reported in Table S1. We generate aggregates of primary cells in which the native architecture of cell complexes is retained (Fig. 1a). We observed dense and well-defined shape spheroids 48h after seeding (Fig. 1b). Immunofluorescence staining revealed positive cells for the epithelial marker, E-cadherin, for CD14, and for αSMA suggesting that patient-derived spheroids retain hepatocytes, Kupffer cells, and hepatic stellate cells, respectively (Fig. 1c, upper and middle pictures). Analysis of the mechanosignaling components showed the presence of F-actin and of the focal adhesion kinase (FAK), key proteins to conduct mechanosignals from the EM into specific intracellular signaling responses modulating cell behavior and function (10, 11) (Fig. 1c, lower picture). Cell viability is high and remains constant up to 8 days (Fig. 1d and 1e). Liver-specific functions, albumin

release and CYP activity, are maintained (Fig. 1f). We detected the release of MIP1a/CCl3 (Fig. 1g), the production of hepatic triglycerides (Fig. 1h), and the deposition of total collagen (Fig. 1i) suggesting functional macrophages (12), endothelial cells (13), and hepatic stellate cells (14, 15). The establishment success rate of our models is 100% independently from the type of liver disease.

HCC tumorspheres show heterogeneous responses to FDA-approved drugs. We assessed the response of HCC tumorspheres to a panel of targeted- and immune-based compounds (Fig. 2a and 2b). Tumorspheres generated from nine HCC patients, showed a heterogeneous response to FDA-approved molecules suggesting inter- and intra-individual tumor characteristics. Drugs (lenvatinib, sorafenib, and regorafenib) that target common signaling pathway (VEGFR) induced similar reduction of cancer cells viability (346, S19, S22, 422). Cabozantinib, a Met tyrosine kinase inhibitor, decreased tumor cells viability in six patients out of nine (S19, S22, 381, 394, 404, 422). Tumorspheres from three patients (S22, S18, 422) were sensitive to immune-check point inhibitors, nivolumab (PD1) and atezolizumab (PDL1). One patient out of nine was resistant to all therapies (S12). To reinforce our model value, we compared the efficacy of bevacizumab, a recombinant humanized monoclonal antibody that binds to soluble VEGFA, preventing receptor binding and inhibiting cell function (16), to sorafenib, a multikinase inhibitor, that targets VEGFR (17). As expected, compounds that target common signaling pathway, although with a different mode of action, mediate similar response in HCC tumorspheres (422 is sensitive while 404 is resistant to both bevacizumab and sorafenib) (Fig. 2b) highlighting the importance of the VEGFR signaling cascade in patient 422. Patients 404 and 381 are sensitive only to cabozantinib suggesting a predominance of tumor-driven MET signaling. Our data demonstrate that the model retains an inter- and intra-heterogeneity of the tumor

microenvironment enabling to investigate differentiated responses to targeted- and immune-based therapies.

High reproducibility of the model enables robust functional analyses following cryopreservation. We investigated the reproducibility of the model by performing a drug efficacy test on tumorspheres generated from fresh and cryopreserved liver tissues, both from the same patient (Fig. 3). Tumorspheres generated from HCC fresh liver tissue (346) that are sensitive to sorafenib, remained sensitive after a cryopreservation period. As control of absence of response of normal primary liver cells to sorafenib (18), we generated spheroids from fresh or from cryopreserved healthy liver tissue (349). We found that those spheroids were insensitive to sorafenib in both conditions. We confirmed that the model is reproducible even from cryopreserved HCC tissues showing similar response/unresponse to sorafenib in two independent experiments with a time interval of 4 months (S12, S19).

Discussion.

We describe a simple model that retains the intrinsic tumor microenvironment allowing the analysis of targeted- and immune-based therapies on the same patient. Our models are differentially sensitive to drugs targeting distinct signaling components, suggesting that they are valuable tools for the discovery of drug mode of action and drug repositioning. The model offers a unique opportunity to assess easily combination therapies helping to identify synergistic sorafenib/bortezomib (19) and additive tivantinib/nivolumab or capmatinib/atezolizumab (20) molecules to accelerate HCC treatment options.

We have successfully generated spheroids from needle liver biopsies (data not shown). However, in this study, we only report data obtained from resected HCC liver tissues as these samples allow to produce a sufficient number of patient-derived spheroids to perform a simultaneous screen of targeted- and immune-based molecules on the same patient for a proof-of-concept study. We're aware that this approach does not allow a retrospective correlation analysis with clinical response because resected patients do not undergo systemic therapies. However, our data emphasize the potential prospective use of our model, that could be prepared from needle liver biopsies, to predict clinical responses enhancing success in finding adequate treatment options. Moreover, strategies to reconstruct the patient's own tumor as tumor organoids, have revealed 88% positive predictive and 100% negative predictive individual response to chemotherapy for patients with colorectal and gastroesophageal cancer (21), and 85% of tumor organoids that incorporate autologous immune cells, showed a treatment response that correlates to the clinical outcome (22). Thus the use of our model to predict clinical treatment response is, at a minimum, as good as using patient-derived organoids, encouraging the development of clinical research programs to accelerate personalized medicine.

HCC retains inter- and intra-tumor heterogeneity, and thus poses tremendous challenges for systemic treatments. In clinical practice, needle liver biopsies are used to clarify diagnosis, to predict prognosis, and to make treatment decisions. This sampling strategy may not fully reflect the intra-tumor heterogeneity and thus may not truly reproduce the clinical outcome. Nevertheless, it has been reported that organoids generated from multiple needle liver biopsies from the same location in a tumor, are mutually representative and are similar to originating tumors (5) suggesting that

patient-derived spheroids generated from needle liver biopsy are representative of the intra-tumor heterogeneity and thus are relevant to predict treatment responses.

We demonstrate that preserving the integrity of the primary tumor architecture enhances the success rate for the generation of HCC tumorspheres. This improvement may occur via the release of soluble factors or through native cell-to-cell contacts that regulate cell vitality (23). However, this action is often masked by the biological function triggered by cell-soluble factor interactions (24). Our model offers a unique opportunity to study the cellular communication within the tumor microenvironment. Further investigation of the tumor secretome would help to understand the degree of implication of direct cell-to-cell communication in the physiopathology of HCC.

Treating hepatic malignancies requires new anticancer molecules. However, clinical trials are costly, time consuming, and most compounds do not reach final criteria (25) because they were incorrectly selected in imperfect models that do not fully recapitulate the physiopathology. Our model offers a substantial add-on basis platform for a better preselection of drug candidates to reduce drastically the cost of drug development enhancing the number of molecules that will reach the end-goal.

In summary, we describe a simple and robust patient-derived model for HCC that retains the tumor heterogeneity and that is fully suitable for implementation into clinical research programs to accelerate personalized medicine. Moreover, the above model will be a valuable tool for the scientific community studying deeper the cellular network within the tumor microenvironment.

References.

1. Bray F, Ferlay J, Soerjomataram I, Siegel RL, Torre LA, Jemal A. Global cancer statistics 2018: GLOBOCAN estimates of incidence and mortality worldwide for 36 cancers in 185 countries. CA Cancer J Clin 2018;68:394-424.

2. Raoul JL, Frenel JS, Raimbourg J, Gilabert M. Current options and future possibilities for the systemic treatment of hepatocellular carcinoma. Hepat Oncol 2019;6:HEP11.

3. Harding JJ, Khalil DN, Abou-Alfa GK. Biomarkers: What Role Do They Play (If Any) for Diagnosis, Prognosis and Tumor Response Prediction for Hepatocellular Carcinoma? Dig Dis Sci 2019;64:918-927.

4. Gillet JP, Varma S, Gottesman MM. The clinical relevance of cancer cell lines. J Natl Cancer Inst 2013;105:452-458.

5. Nuciforo S, Fofana I, Matter MS, Blumer T, Calabrese D, Boldanova T, Piscuoglio S, et al. Organoid Models of Human Liver Cancers Derived from Tumor Needle Biopsies. Cell Rep 2018;24:1363-1376.

6. Deville SS, Cordes N. The Extracellular, Cellular, and Nuclear Stiffness, a Trinity in the Cancer Resistome-A Review. Front Oncol 2019;9:1376.

7. Baker K. Organoids Provide an Important Window on Inflammation in Cancer. Cancers (Basel) 2018;10.

8. Blumer T, Fofana I, Matter MS, Wang X, Montazeri H, Calabrese D, Coto-Llerena M, et al. Hepatocellular Carcinoma Xenografts Established From Needle Biopsies Preserve the Characteristics of the Originating Tumors. Hepatol Commun 2019;3:971-986.

9. Ben-David U, Ha G, Tseng YY, Greenwald NF, Oh C, Shih J, McFarland JM, et al. Patient-derived xenografts undergo mouse-specific tumor evolution. Nat Genet 2017;49:1567-1575.

10. Northey JJ, Przybyla L, Weaver VM. Tissue Force Programs Cell Fate and Tumor Aggression. Cancer Discov 2017;7:1224-1237.

11. Shivashankar GV. Mechanosignaling to the cell nucleus and gene regulation. Annu Rev Biophys 2011;40:361-378.

12. Ntanasis-Stathopoulos I, Fotiou D, Terpos E. CCL3 Signaling in the Tumor Microenvironment. Adv Exp Med Biol 2020;1231:13-21.

13. Adams DH, Hubscher S, Fear J, Johnston J, Shaw S, Afford S. Hepatic expression of macrophage inflammatory protein-1 alpha and macrophage inflammatory protein-1 beta after liver transplantation. Transplantation 1996;61:817-825.

14. Kim BM, Abdelfattah AM, Vasan R, Fuchs BC, Choi MY. Hepatic stellate cells secrete Ccl5 to induce hepatocyte steatosis. Sci Rep 2018;8:7499.

15. Shang L, Hosseini M, Liu X, Kisseleva T, Brenner DA. Human hepatic stellate cell isolation and characterization. J Gastroenterol 2018;53:6-17.

16. Ranieri G, Patruno R, Ruggieri E, Montemurro S, Valerio P, Ribatti D. Vascular endothelial growth factor (VEGF) as a target of bevacizumab in cancer: from the biology to the clinic. Curr Med Chem 2006;13:1845-1857.

17. Adnane L, Trail PA, Taylor I, Wilhelm SM. Sorafenib (BAY 43-9006, Nexavar), a dual-action inhibitor that targets RAF/MEK/ERK pathway in tumor cells and tyrosine kinases VEGFR/PDGFR in tumor vasculature. Methods Enzymol 2006;407:597-612.

18. Zhao X, Tian C, Puszyk WM, Ogunwobi OO, Cao M, Wang T, Cabrera R, et al. OPA1 downregulation is involved in sorafenib-induced apoptosis in hepatocellular carcinoma. Lab Invest 2013;93:8-19.

19. Chen KF, Yu HC, Liu TH, Lee SS, Chen PJ, Cheng AL. Synergistic interactions between sorafenib and bortezomib in hepatocellular carcinoma involve PP2A-dependent Akt inactivation. J Hepatol 2010;52:88-95.

20. Li H, Li CW, Li X, Ding Q, Guo L, Liu S, Liu C, et al. MET Inhibitors Promote Liver Tumor Evasion of the Immune Response by Stabilizing PDL1. Gastroenterology 2019;156:1849-1861 e1813.

21. Yan HHN, Siu HC, Law S, Ho SL, Yue SSK, Tsui WY, Chan D, et al. A Comprehensive Human Gastric Cancer Organoid Biobank Captures Tumor Subtype Heterogeneity and Enables Therapeutic Screening. Cell Stem Cell 2018;23:882-897 e811.

22. Votanopoulos KI, Forsythe S, Sivakumar H, Mazzocchi A, Aleman J, Miller L, Levine E, et al. Model of Patient-Specific Immune-Enhanced Organoids for Immunotherapy Screening: Feasibility Study. Ann Surg Oncol 2020;27:1956-1967.

23. Pavel M, Renna M, Park SJ, Menzies FM, Ricketts T, Fullgrabe J, Ashkenazi A, et al. Contact inhibition controls cell survival and proliferation via YAP/TAZ-autophagy axis. Nat Commun 2018;9:2961.

24. Nelson CM, Chen CS. Cell-cell signaling by direct contact increases cell proliferation via a PI3K-dependent signal. FEBS Lett 2002;514:238-242.

25. Wong CH, Siah KW, Lo AW. Estimation of clinical trial success rates and related parameters. Biostatistics 2019;20:273-286.

Figure 1

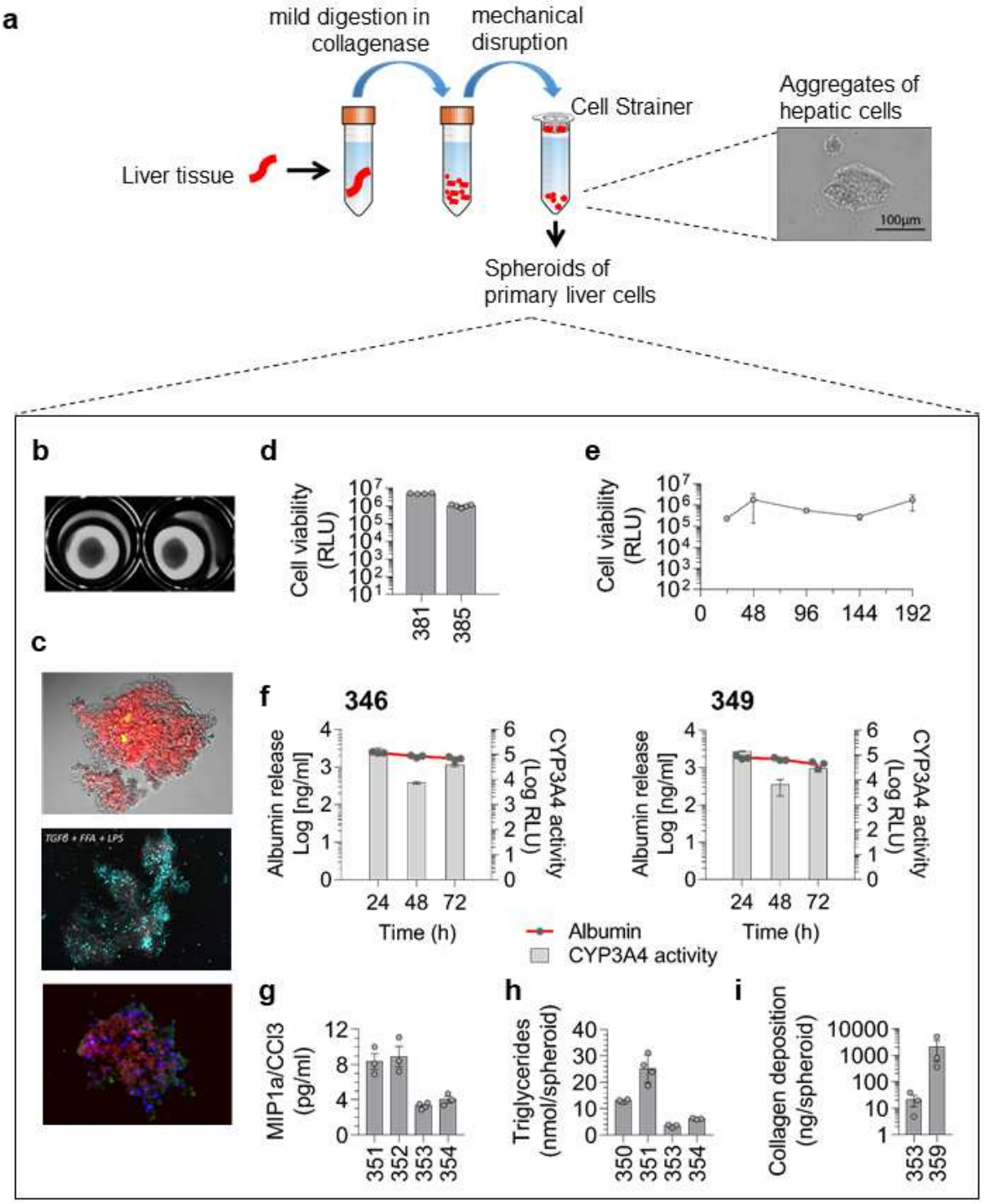

Fig. 1. Patient-derived spheroids retain functional liver microenvironment. (a) Workflow for the generation of patient-derived spheroids from resected liver tissues. The picture shows primary hepatic cell clusters after size filtering. (b) Well-defined architecture of patient-derived spheroids at day 2. (c) Characterization of liver

spheroids by immunofluorescence. Upper photo, E-cadherin (red) and CD14 (green) staining. Middle photo, αSMA (red) and nuclei (blue) staining after 24h of treatment with TGFβ+FFA+LPS. Lower photo, F-actin (red), FAK (green), and nuclei (blue) staining. (d) Cell viability after 6 days of culture. (e) Cell viability lasts up to 8 days. The kinetic of cell viability was measured. Results (n=3) from patient 373 are shown as mean ± s.d. of relative luminescence unit (RLU). (f) Hepatic function assessment. Albumin release and CYP activity were measured at 24h, 48, and 72h. Results are shown as mean ± s.d. of RLU for CYP activity and as Log[ng/ml] for albumin. (g) Quantification of MIP1a/CCl3 release at day 6. (h) Triglycerides amount after 6 days of culture. (i) Total collagen deposition at day 12. A minimum of triplicates were performed for each patient.

Figure 2

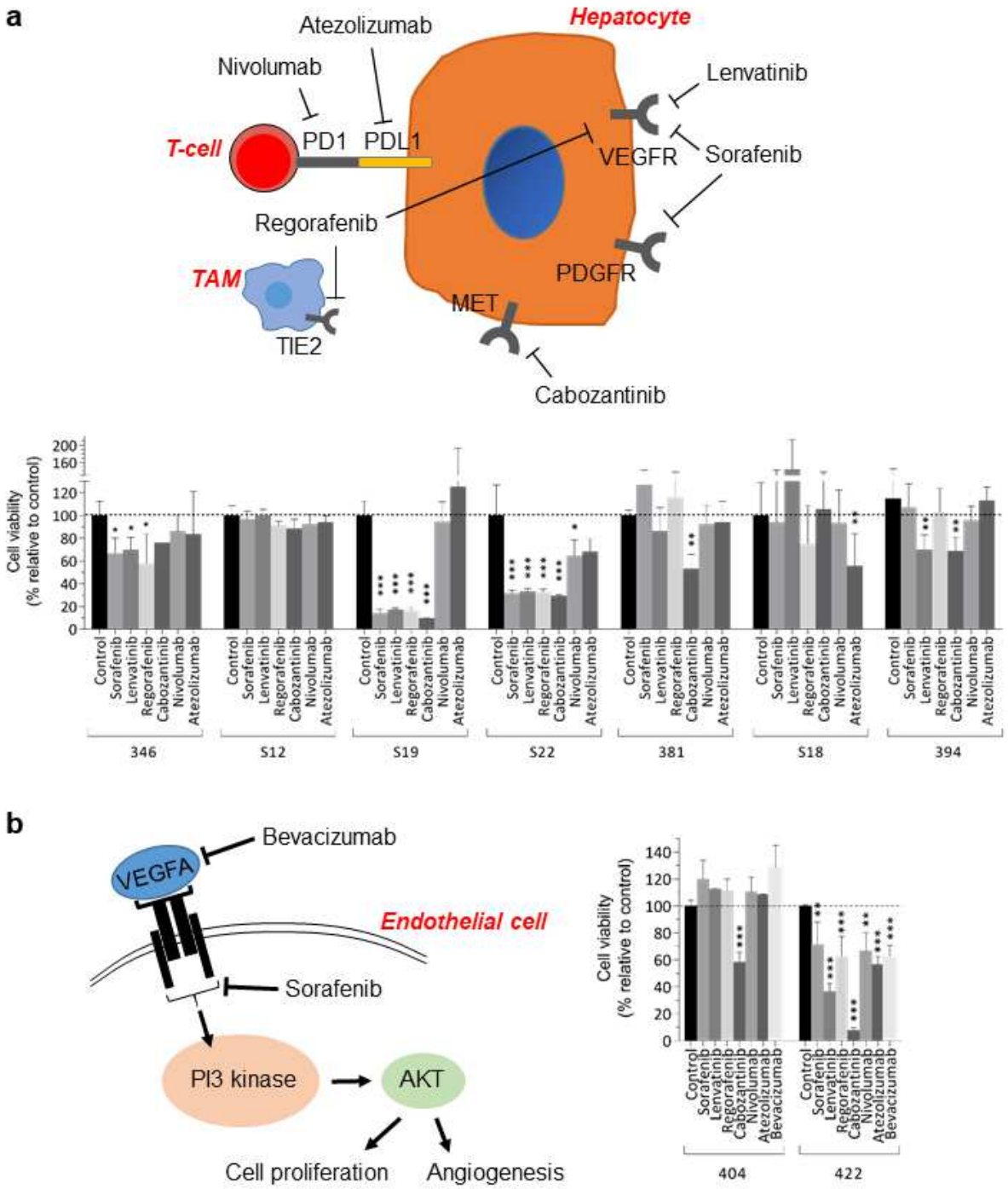

Fig. 2. Tumorspheres retain inter- and intra-heterogeneity sensitivity to FDA-approved drugs. (a) Scheme showing targeted- and immune-based drugs and their therapeutic targets. Tumorspheres were generated from tumor tissues from seven HCC patients and then treated with FDA-approved drugs. (b) Scheme showing

therapeutic targets of bevacizumab and of sorafenib. Tumorspheres from two HCC patients were treated for 6 days. Cell viability was measured. Results are expressed as percentage of viable cells to control and shown as mean ± s.d. A minimum of triplicates were performed for each condition.

Figure 3

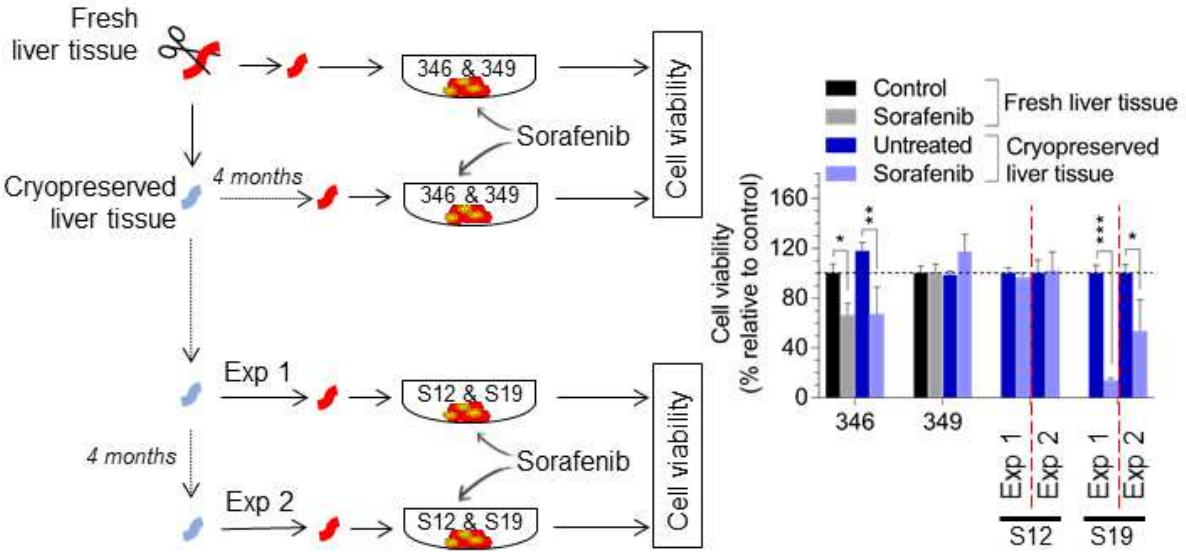

Fig. 3. The model is highly reproducible for drug response assessment. Resected liver tissues were divided into 2 fragments immediately after collection. One piece was used immediately to generate spheroids and the other one was cryopreserved for 4 months before being used to generate spheroids (346-HCC and 349-Healthy tissue). Cryopreserved HCC tissues (S12 and S19) were used to generate tumorspheres in two independent experimental settings in a four-months interval. Tumorspheres were treated with sorafenib for 6 days and cell viability monitored. Results are expressed as percentage of viable cells to control and shown as mean ± s.d. A minimum of triplicates were performed for each condition.

ID	Surgical indication	Chronic Liver disease	Staging	HCC Grading (Edmondson-Steiner)	Miscellaneous
346	HCC	No	F1	G1-G2	Macrophage infiltration, portal embolization
349	CCM	No	F1	G1	Macrophage infiltration, portal embolization
350	Adenoma	ALD	F4	NA	
351	CCM	NAFL	F0	NA	Colon cancer metastasis
352	CCM	No	F1	NA	Sinusoidal congestion
353	CCM	No	F0	NA	Macrophage infiltration, liver embolization
354	CCM	NASH	F0	NA	Neo-adjuvant chimiotherapy
359	RGN	NASH	F4	NA	
373	ICC	NAFL	F0	NA	
381	HCC	ALD	F1-F2	G2	
385	Adenoma	ALD	F0	NA	
394	HCC	No	F0-F1	G4	
404	HCC	HCV treated and ALD	F1-F2	G1	
422	HCC	HCV treated	F4	G1	
S12	HCC	NASH	F4	G1-G2	
S18	HCC	HCV	F2-F3	G2-G3	
S19	HCC	NASH	F4	G2	
S22	HCC	NASH	F2-F3	G1-G2	

ALD = Alcoholic Liver Disease, CCM= colon cancer metastasis, NA= not applicable, NAFL=non-alcoholic fatty liver, NASH= non-alcoholic steatohepatitis
RGN= regenerative nodule

Table 1. Characteristics of liver tissues that are included in the study. Liver tissues were collected with written informed consent from patients and were immediately stored in a hypothermal solution (HypoThermosol FRS Preservation Solution, Sigma-Aldrich) prior processing or cryopreserved in CryoStor® cell cryopreservation media (Sigma-Aldrich).

Figures

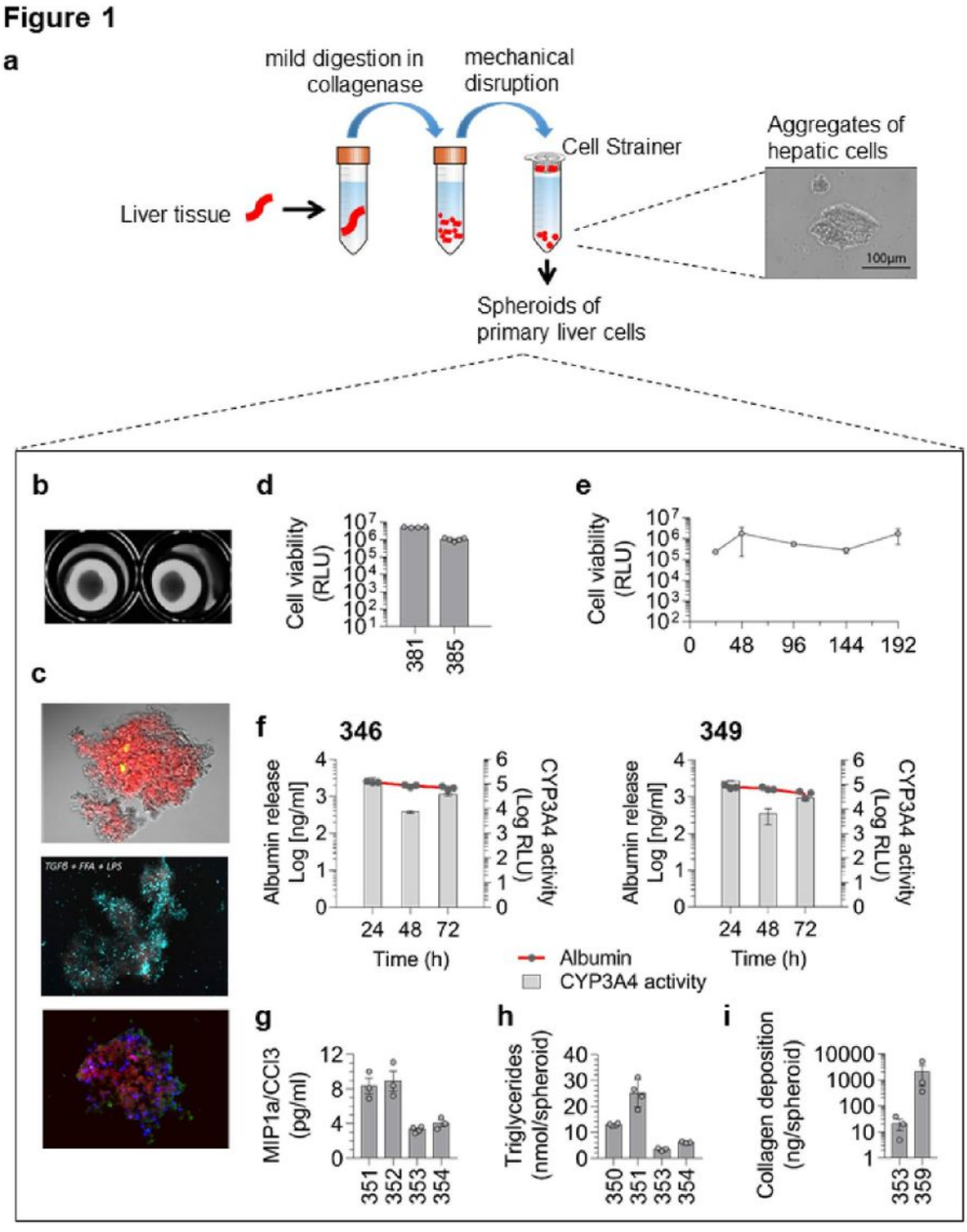

Figure 1

Patient-derived spheroids retain functional liver microenvironment. (a) Workflow for the generation of patient-derived spheroids from resected liver tissues. The picture shows primary hepatic cell clusters after size filtering. (b) Well-defined architecture of patient-derived spheroids at day 2. (c) Characterization of

liver spheroids by immunofluorescence. Upper photo, E-cadherin (red) and CD14 (green) staining. Middle photo, αSMA (red) and nuclei (blue) staining after 24h of treatment with TGFβ+FFA+LPS. Lower photo, F-actin (red), FAK (green), and nuclei (blue) staining. (d) Cell viability after 6 days of culture. (e) Cell viability lasts up to 8 days. The kinetic of cell viability was measured. Results (n=3) from patient 373 are shown as mean ± s.d. of relative luminescence unit (RLU). (f) Hepatic function assessment. Albumin release and CYP activity were measured at 24h, 48, and 72h. Results are shown as mean ± s.d. of RLU for CYP activity and as Log[ng/ml] for albumin. (g) Quantification of MIP1a/CCl3 release at day 6. (h) Triglycerides amount after 6 days of culture. (i) Total collagen deposition at day 12. A minimum of triplicates were performed for each patient.

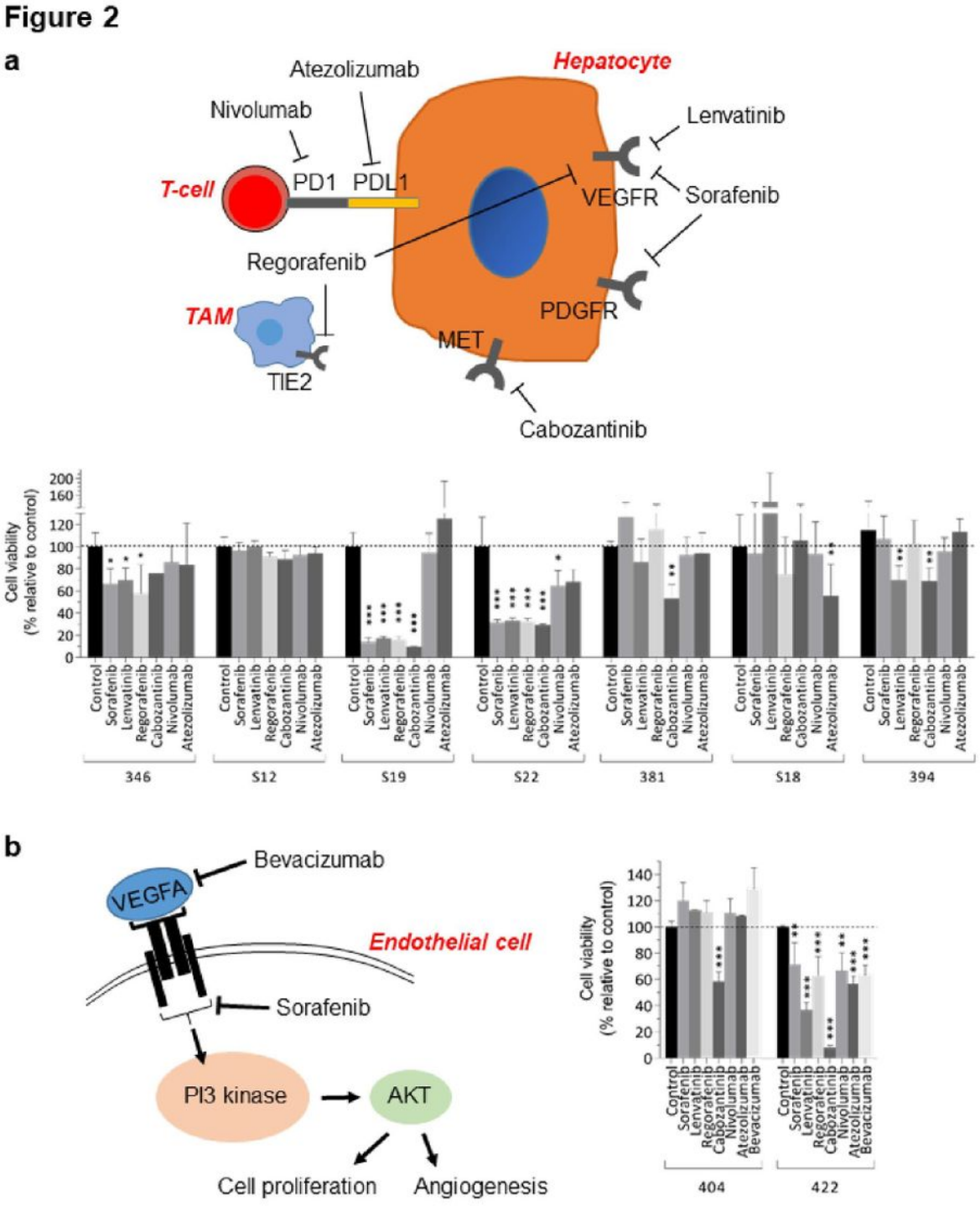

Figure 2

Tumorspheres retain inter- and intra-heterogeneity sensitivity to FDA approved drugs. (a) Scheme showing targeted- and immune-based drugs and their therapeutic targets. Tumorspheres were generated from tumor tissues from seven HCC patients and then treated with FDA-approved drugs. (b) Scheme showing therapeutic targets of bevacizumab and of sorafenib. Tumorspheres from two HCC patients

were treated for 6 days. Cell viability was measured. Results are expressed as percentage of viable cells to control and shown as mean ± s.d. A minimum of triplicates were performed for each condition.

Figure 3

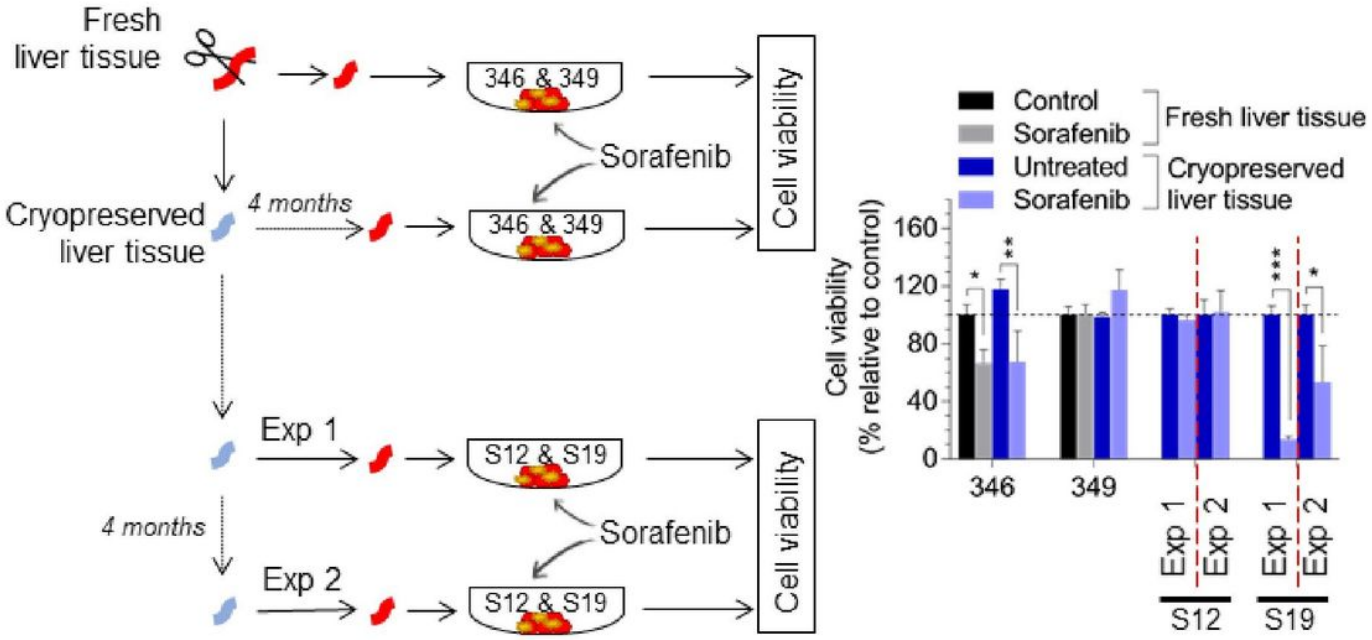

Figure 3

The model is highly reproducible for drug response assessment. Resected liver tissues were divided into 2 fragments immediately after collection. One piece was used immediately to generate spheroids and the other one was cryopreserved for 4 months before being used to generate spheroids (346-HCC and 349-Healthy tissue). Cryopreserved HCC tissues (S12 and S19) were used to generate tumorspheres in two independent experimental settings in a four-months interval. Tumorspheres were treated with sorafenib for 6 days and cell viability monitored. Results are expressed as percentage of viable cells to control and shown as mean ± s.d. A minimum of triplicates were performed for each condition.

Supplementary Files

This is a list of supplementary files associated with this preprint. Click to download.

- GraphicalAbstarct.jpg